

Electronic Supplementary Information for:
Multiple Binding Modes of an Unconjugated Bis(pyridine)
Ligand Stabilize Low-Valent [Cp*Rh] Complexes

Davide Lionetti,^a Victor W. Day,^a Benedikt Lassalle-Kaiser,^{b,*} and James D. Blakemore^{a,*}

^a Department of Chemistry, University of Kansas, 1251 Wescoe Hall Drive,
Lawrence, Kansas 66045, United States

^b Synchrotron Soleil, L'Orme des Merisiers, Saint-Aubin BP 48,
91192 Gif-sur-Yvette Cedex, France

*E-mail: blakemore@ku.edu (J.D.B.); benedikt.lassalle@synchrotron-soleil.fr (B.L.-K.)

Contents

General Considerations	S3
<i>Electrochemistry</i>	S3
<i>X-Ray Absorption Spectroscopy (XAS)</i>	S4
Synthetic Procedures	S5
<i>Synthesis of 3-Cl.</i>	S5
<i>Reduction of 3-Cl.</i>	S5
<i>Generation of 4.</i>	S5
<i>Synthesis of 5.</i>	S6
Figure S1. Numbering scheme for complex 5.	S6
Electrochemistry	S7
Figure S2. CV data for 5.	S7
Figure S3. CV data for 3-CH ₃ CN	S7
Figure S4. CV data for 3-Cl	S8
UV-Vis Spectra	S9
Figure S5. UV-Vis spectrum of 3-Cl in CH ₃ CN	S9
Figure S6. UV-Vis spectrum of 4 in CH ₃ CN	S10
Figure S7. UV-Vis spectrum [Cp*RhCl] ₂	S11
Figure S8. UV-Vis spectrum of 5 in THF.	S11
NMR Spectra	S13
Figure S9. ¹ H NMR spectrum of 3-Cl	S13
Figure S10. ¹³ C { ¹ H} NMR spectrum of 3-Cl	S13
Figure S11. ¹⁹ F NMR spectrum of 3-Cl	S14
Figure S12. ³¹ P { ¹ H} NMR spectrum of 3-Cl	S14
Figure S13. NOESY spectrum of 3-Cl	S15
Figure S14. ¹ H NMR spectrum of 3-CH ₃ CN	S16
Figure S15. ¹ H NMR spectrum of [Cp*RhCl] ₂	S16

Figure S16. ^1H NMR spectrum of 4	S17
Figure S17. ^1H NMR spectrum of 5	S18
Figure S18. $^{13}\text{C}\{^1\text{H}\}$ NMR spectrum of 5	S18
Figure S19. COSY spectrum of 5	S19
Figure S20. HSQC spectrum of 5	S20
Figure S21. HMBC spectrum of 5	S21
Figure S22. NOESY spectrum of 5	S22
Crystallographic Information	S23
<i>Refinement Details</i>	S23
Table S1. Crystal and Refinement Data	S24
Refinement Details for 3-Cl.	S25
Figure S23. Full solid-state structure of 3-Cl.	S25
Refinement Details for 4.	S26
Figure S24. Full solid-state structure of 4	S27
Refinement Details for 5.	S28
Figure S25. Full solid-state structure of 5.	S28
Table S2. Relevant structural parameters	S29
References	S30

General Considerations

All manipulations were carried out in dry N₂-filled gloveboxes (Vacuum Atmospheres Co., Hawthorne, CA) or under N₂ atmosphere using standard Schlenk techniques unless otherwise noted. All solvents were of commercial grade and dried over activated alumina using a PPT Glass Contour (Nashua, NH) solvent purification system prior to use, and were stored over molecular sieves. All chemicals were from major commercial suppliers and used as received after extensive drying. [Cp*RhCl₂]₂ and dimethyldipyridylmethane (Me₂dpma) were prepared according to literature procedures.¹ Deuterated NMR solvents were purchased from Cambridge Isotope Laboratories; CD₃CN was dried over 3-Å molecular sieves and C₆D₆ was dried over sodium/benzophenone. ¹H, ¹³C, ¹⁹F, and ³¹P NMR spectra were collected on 400 or 500 MHz Bruker spectrometers and referenced to the residual protio-solvent signal² in the case of ¹H and ¹³C. Heteronuclear NMR spectra were referenced to the appropriate external standard following the recommended scale based on ratios of absolute frequencies (Ξ).³ ¹⁹F NMR spectra are reported relative to CCl₃F, and ³¹P NMR spectra are reported relative to H₃PO₄. Chemical shifts (δ) are reported in units of ppm and coupling constants (*J*) are reported in Hz. Electronic absorption spectra were collected with an Ocean Optics Flame spectrometer, in a 1 cm pathlength quartz cuvette. Elemental analyses were performed by Midwest Microlab, Inc. (Indianapolis, IN).

Electrochemistry

Electrochemical experiments were carried out in a nitrogen-filled glovebox. 0.10 M tetra(*n*-butylammonium) hexafluorophosphate (Sigma-Aldrich; electrochemical grade) in acetonitrile served as the supporting electrolyte. Measurements were made with a Gamry Reference 600 Plus Potentiostat/Galvanostat using a standard three-electrode configuration. The working electrode was the basal plane of highly oriented pyrolytic graphite (HOPG) (GraphiteStore.com, Buffalo Grove, Ill.; surface area: 0.09 cm²), the counter electrode was a platinum wire (Kurt J. Lesker, Jefferson Hills, PA; 99.99%, 0.5 mm diameter), and a silver wire immersed in electrolyte served as a pseudo-reference electrode (CH Instruments). The reference was separated from the working solution by a Vycor frit (Bioanalytical Systems, Inc.). Ferrocene (Sigma Aldrich; twice-sublimed) was added to the electrolyte solution at the conclusion of each experiment (~1 mM); the midpoint potential of the ferrocenium/ferrocene couple (denoted as Fc⁺⁰) served as an external standard for comparison of the recorded potentials. Concentrations of analyte for cyclic voltammetry were typically 2 mM.

X-Ray Absorption Spectroscopy (XAS)

XAS spectra were collected on the LUCIA beamline of the SOLEIL Synchrotron, with a ring energy of 2.75 GeV and an operating current of 500 mA. The incoming energy was monochromatized using a double crystal Si(111) monochromator and the data were collected in fluorescence mode using a Bruker silicon drift detector. In order to avoid self-absorption, samples were prepared as 5% weight/weight graphite pellets and data were recorded using an outgoing grazing angle of 5°. Samples were prepared in an argon glovebox and transferred to the beamline in an argon filled sealed vessel. Data collection was then performed under the primary vacuum of the LUCIA measurement chamber. XAS data were normalized to the incident flux and calibrated with respect to a titanium foil (4966 eV). 10 scans were typically recorded and averaged for each sample and the resulting spectra were normalized to an edge jump of 1. No radiation damage could be observed on these samples with the measurement conditions we used.

Synthetic Procedures

Synthesis of **3-Cl**.

To a suspension of $[\text{Cp}^*\text{RhCl}_2]_2$ in CH_3CN (0.3197 g, 0.517 mmol) were added Me_2dpma (0.2051 g, 1.03 mmol, 2 equiv) and AgPF_6 (0.2616 g, 1.03 mmol, 2 equiv) as CH_3CN solutions. The color of the reaction mixture rapidly changed from brick-red to yellow-orange, and a colorless precipitate formed. After 30 min, the suspension was filtered to remove the AgCl byproduct, and the volume of the filtrate was reduced to ~ 2 mL. Addition of Et_2O (~ 100 mL) caused precipitation of a yellow solid, which was collected by filtration (0.591 g, 93%). Single-crystals suitable for X-ray diffraction studies were obtained by vapor diffusion of Et_2O into a concentrated CH_3CN solution of the title compound. ^1H NMR (500 MHz, CD_3CN) δ 8.84 (dd, $J = 5.7, 1.7$ Hz, 2H, *o*-PyH), 8.01 (ddd, $J = 8.3, 7.5, 1.8$ Hz, 2H, *p*-PyH), 7.78 (d, $J = 8.2$ Hz, 2H), 7.45 (ddd, $J = 7.3, 5.7, 1.4$ Hz, 2H, *m*-PyH), 2.06 (s, 3H, *exo*-C(CH_3)), 1.89 (s, 3H, *endo*-C(CH_3)), 1.60 (s, 15H, $\text{C}_5(\text{CH}_3)_5$) ppm. ^{13}C NMR (126 MHz, CD_3CN) δ 164.0, 157.9 (d, $^2J_{\text{C,Rh}} = 1.8$ Hz), 141.3, 125.5, 123.8, 98.9 (d, $^1J_{\text{C,Rh}} = 8.4$ Hz, Rh-C $_5(\text{CH}_3)_5$), 47.4 (d, $^3J_{\text{C,Rh}} = 1.7$ Hz, C(CH_3) $_2$), 29.0 (C(CH_3)), 27.7 (C(CH_3)), 9.5 (Rh-C $_5(\text{CH}_3)_5$) ppm. ^{19}F NMR (376 MHz, CD_3CN) δ -73.0 (d, $^1J_{\text{F,P}} = 706$ Hz) ppm. ^{31}P NMR (162 MHz, CD_3CN) δ -142.5 (sept, $^1J_{\text{P,F}} = 706$ Hz) ppm. Electronic absorption spectrum (CH_3CN): 206 (28,200), 240 (26,000), 267 (11,600; sh), 373 (2,700), 420 nm ($2,200 \text{ M}^{-1} \text{ cm}^{-1}$). Anal. Calcd. for $\text{C}_{23}\text{H}_{29}\text{ClF}_6\text{N}_2\text{PRh}$: C, 44.79; H, 4.74; N, 4.54. Found: C, 44.83; H, 4.77; N, 4.52.

Reduction of **3-Cl**.

Attempts at chemical reduction of **3-Cl** with CoCp_2 (1 equiv) resulted in generation of a deep blue solution. Extraction of the dark residue with Et_2O yielded a blue solid; ^1H NMR (C_6D_6 , 400 MHz) analysis of this material revealed a singlet at 1.60 ppm. The ^1H NMR data and the blue color of the compound (see Figures S6 and S14) match literature reports⁴ of the dimeric Rh(II) species $[\text{Cp}^*\text{RhCl}]_2$ —a diamagnetic compound due to the presence of a Rh–Rh bond. We thus conclude that, under our conditions, one-electron reduction of **3-Cl** results in loss of the Me_2dpma ligand and leads to generation of $[\text{Cp}^*\text{RhCl}]_2$. Consistent with this assignment, XRD data on crystals of this blue species (unit cell parameters) match those observed previously for $[\text{Cp}^*\text{RhCl}]_2$.⁴ Retention of the bis(pyridyl) ligand upon reduction of the Rh(III) species in the absence of a halide anion (*vide infra*) suggests that generation of the Rh(II) dimer is driven by the ability of halide ligands to engage in a bridging interaction between the two metal centers in the dimer.

In accord with this chemical work, the electrochemical behavior of **3-Cl** is complex and difficult to deconvolute, due to the presence of chloride (see Figure S3). Therefore, most electrochemical studies were carried out following abstraction of the Cl^- ligand according to the procedure described below.

Generation of **4**.

To a yellow-orange solution of **3-Cl** in CH_3CN (0.0989 g, 0.160 mmol) was added AgPF_6 (0.0404 g, 0.160 mmol, 1 equiv) in CH_3CN . The color of the solution lightened slightly, and a colorless precipitate formed immediately. The mixture was stirred for 30 min; it was then filtered through Celite and the volatiles removed *in vacuo*. The yellow solid thus obtained was analyzed by ^1H NMR to confirm full conversion of **3-Cl** to **3-CH₃CN**. ^1H NMR (400 MHz, CD_3CN) δ 8.86 (dd, $J = 5.8, 1.7$ Hz, 2H), 8.14 (ddd, $J = 8.3, 7.3, 1.7$ Hz, 2H), 7.95

(dd, $J = 8.3, 1.6$ Hz) 2H,, 7.62 (ddd, $J = 7.3, 5.7, 1.5$ Hz 2H,), 2.17 (s, 3H, Rh-NCCH₃), 2.10 (s, 3H, C(CH₃)), 1.79 (s, 3H, C(CH₃)), 1.68 (s, 15H, C(CH₃)₅) ppm.

To prepare reduced species **4**, a portion of this material (0.0472 g, 0.0615 mmol) was treated with CoCp₂ (0.0116 g, 0.0615 mmol, 1 equiv) in CH₃CN. The solution color changed immediately from yellow to dark purple. The volatiles were removed *in vacuo* to obtain a dark purple solid. ¹H NMR analysis of this material shows only a signal consistent with diamagnetic [CoCp₂][PF₆] (δ 5.67 ppm in CD₃CN); complex **4** is silent by ¹H NMR. Electronic absorption spectrum (CH₃CN): 522 (2900), 700-750 nm (\sim 400 M⁻¹ cm⁻¹). Single-crystals of **4** were grown via vapor diffusion of Et₂O into a CH₃CN solution of the product mixture containing **4** and [CoCp₂][PF₆]. The resulting dark purple crystals were used for XRD studies.

Synthesis of **5**.

A suspension of **3-Cl** in THF (0.2635 g, 0.426 mmol) was stirred over freshly prepared sodium-mercury amalgam (1% Na in Hg; 0.0979 g Na⁰, 4.26 mmol, 10 equiv) for 6 hours, during which time the yellow suspension became a dark red homogeneous solution. The mixture was filtered and the volatiles removed *in vacuo*. The crude product mixture contains only two components – the desired reduced compound (**5**) and small amounts (5-10%) of free Me₂dpma ligand. The latter can be separated from the desired product by washing the crude material with hexanes and filtering through a Celite pad. Extraction with Et₂O and removal of the volatiles *in vacuo* provides the title compound as a dark red solid (0.103 g, 55%). Depending on the purity of the hexanes fraction, additional pure material can be obtained via crystallization by cooling the hexanes solution to -35°C. The same strategy was employed using pure material to obtain single-crystals of the title compound suitable for X-ray diffraction studies. ¹H NMR (400 MHz, C₆D₆) δ 8.43 – 8.35 (m, 2H, H1+H13), 7.38 (ddd, $J = 8.5, 6.5, 1.9$ Hz, 1H, H11), 6.73 (td, $J = 7.7, 1.6$ Hz, 1H, H2), 6.47 (dt, $J = 8.0, 1.2$ Hz, 1H, H4), 6.25 (ddd, $J = 7.3, 5.7, 1.5$ Hz, 1H, H3), 6.08 (dd, $J = 8.4, 3.4$ Hz, 1H, H12), 2.25 (dd, $J = 6.5, 1.8$ Hz, 1H, H10), 2.01 (s, 3H, H7), 1.52 (s, 15H, C₅(CH₃)₅), 1.16 (s, 3H, H8). ¹³C NMR (126 MHz, C₆D₆) δ 171.8 (C5), 151.1 (C1), 145.2 (C13), 145.0 (C11), 133.1 (C2), 121.4 (C4), 120.7 (C3), 110.89 (C12), 90.9 (d, ¹J_{C,Rh} = 16.8 Hz, C9), 90.7 (d, ¹J_{C,Rh} = 5.8 Hz, C₅(CH₃)₅), 54.5 (C6), 48.5 (d, ¹J_{C,Rh} = 12.8 Hz, C10), 27.9 (C7), 26.31 (C8), 8.64 (C₅(CH₃)₅) ppm. Electronic absorption spectrum (THF): 247 (16,900), 299 (11,400), 339 (5,300), 503 nm (3,400 M⁻¹ cm⁻¹). Anal. Calcd. for C₂₃H₂₉N₂Rh: C, 63.30; H, 6.70; N, 6.42. Found: C, 63.75; H, 6.60; N, 6.19.

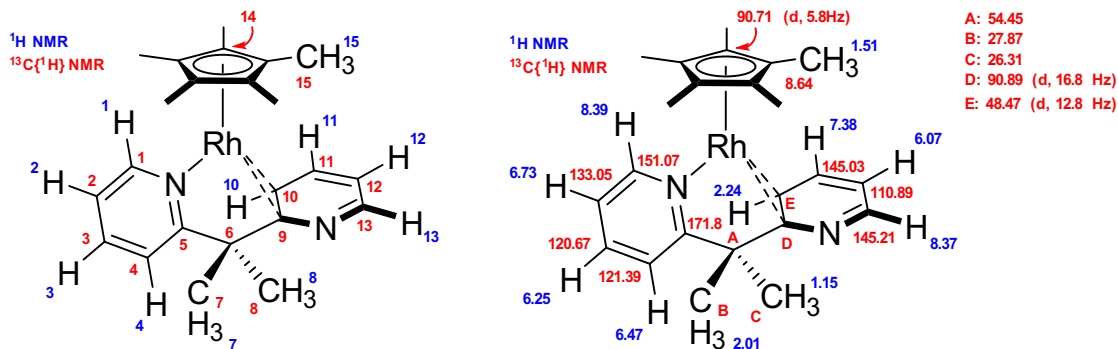


Figure S1. Left: numbering scheme for assignment of NMR data for complex **5**. Right: full assignment of ¹H and ¹³C{¹H} NMR data for **5**.

Electrochemistry

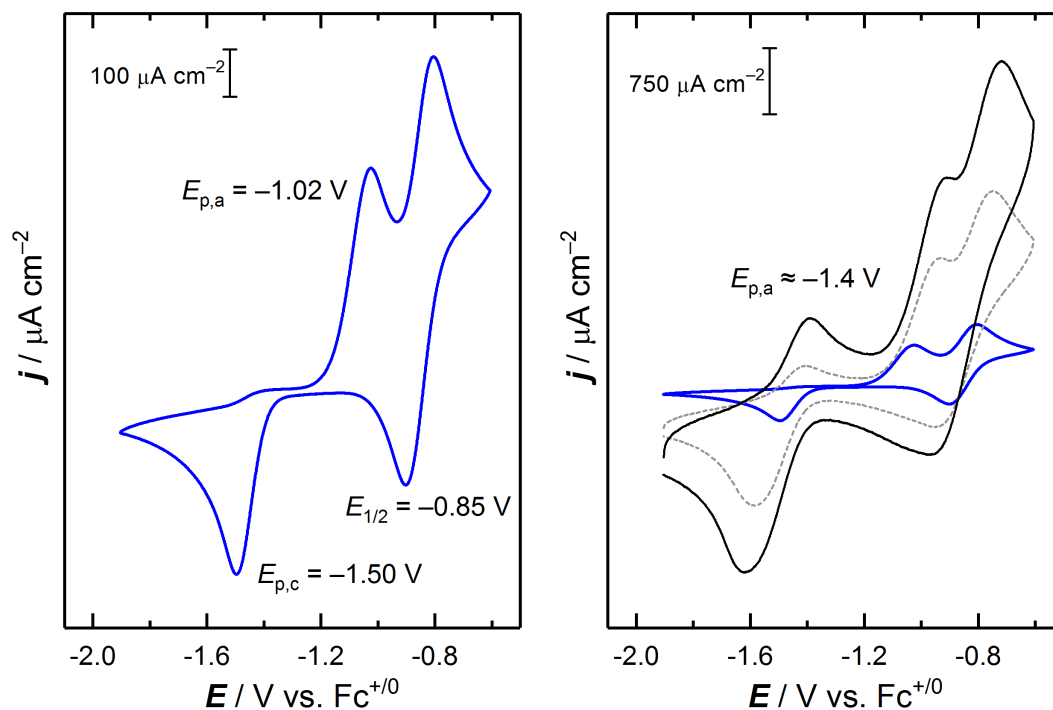


Figure S2. Left: cyclic voltammetry data for complex **5** in CH_3CN (0.1 M $[\text{nBu}_4\text{N}][\text{PF}_6]$, 100 mV/s). Right: comparison of CV data for complex **5** at 100 mV s^{-1} (blue), 1,500 mV s^{-1} (grey, dashed), and 4,000 mV s^{-1} (black).

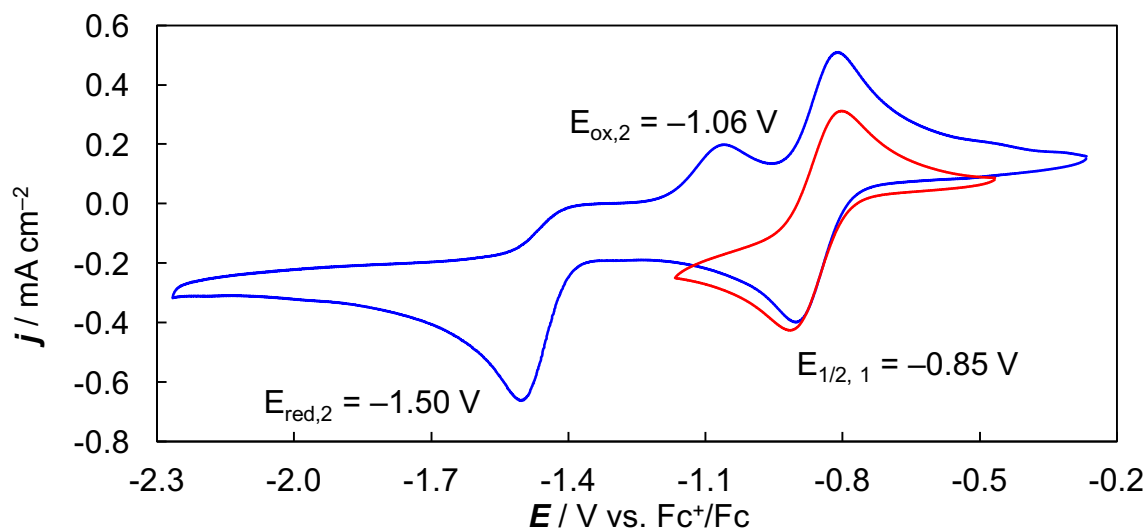


Figure S3. Blue: full cyclic voltammetry data for complex **3-CH₃CN**; red: cyclic voltammetry data for virtually reversible couple at $-0.85\text{ V vs. Fc}^+/\text{Fc}^0$.

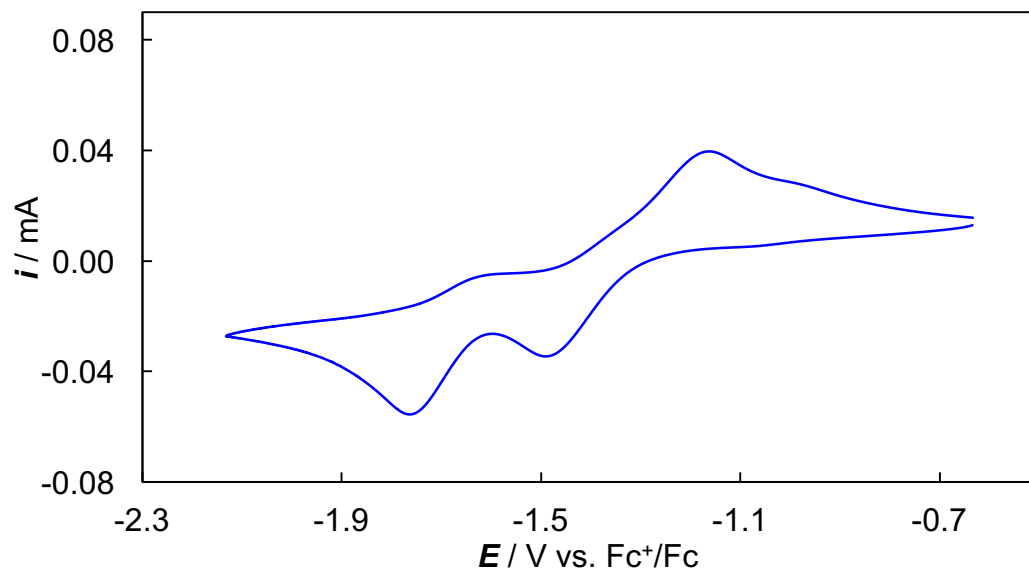


Figure S4. Cyclic voltammetry data for complex **3-Cl** in CH₃CN (0.1 M [ⁿBu₄N][PF₆], 100 mV/s).

UV-Vis Spectra

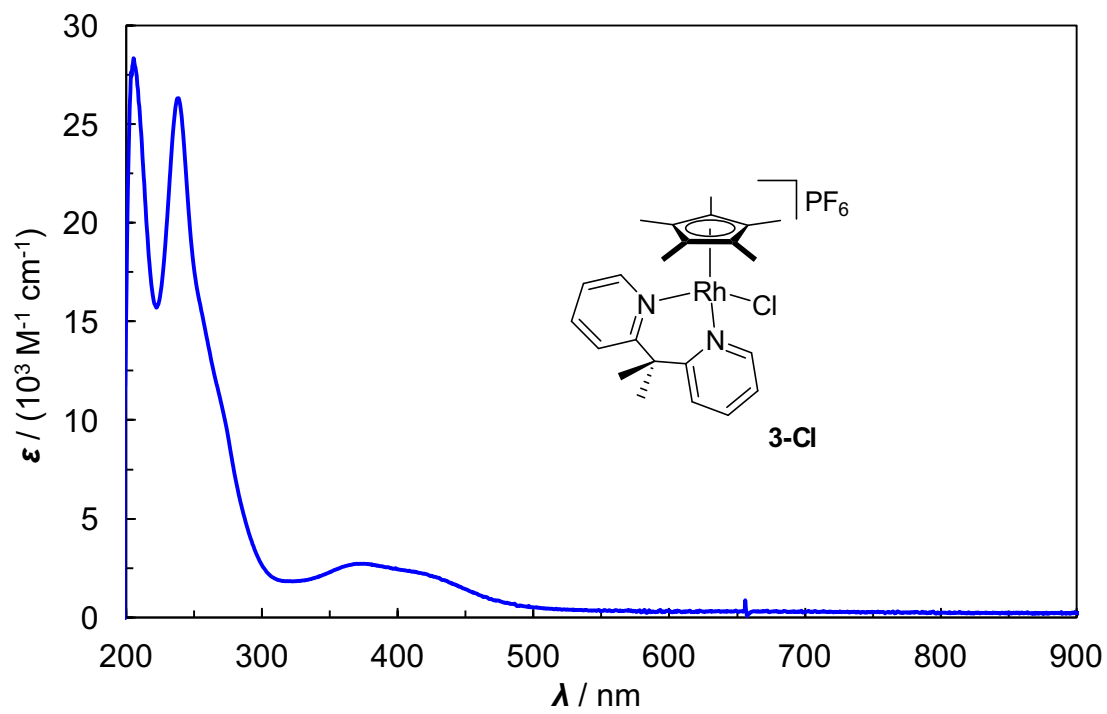


Figure S5. UV-Vis spectrum of **3** in THF.

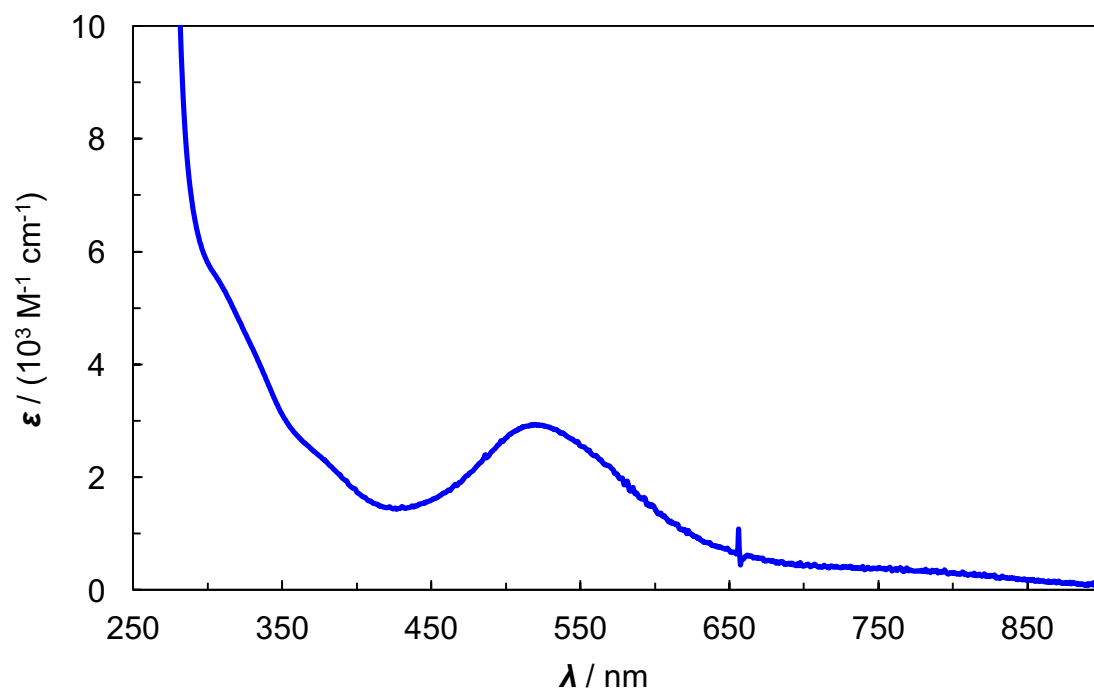
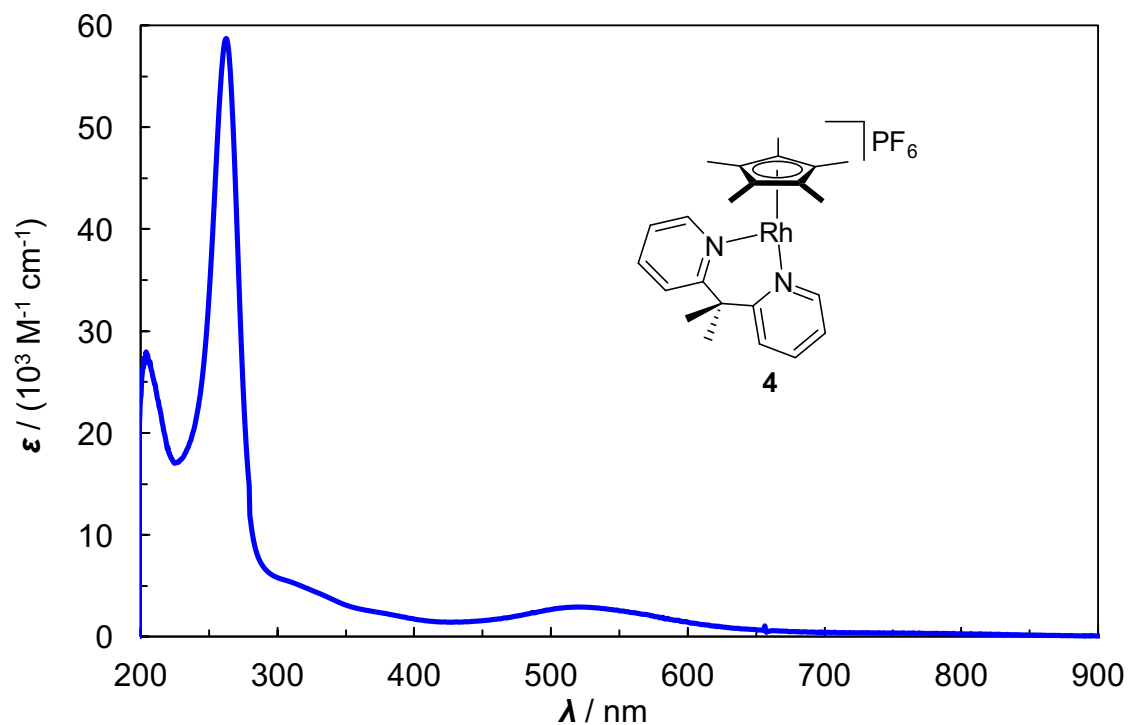


Figure S6. Upper: UV-Vis spectrum in CH_3CN of product mixture from treatment of **3**- CH_3CN with CoCp_2 . Molar absorptivity was calculated on the basis of 1:1 mixture of Rh(II) species **3** and $[\text{CoCp}_2][\text{PF}_6]$. Based on the known absorbance profile for $[\text{CoCp}_2]^+$,⁵ absorptions at wavelengths longer than 450 nm can confidently be assigned to **4**. Lower: expanded view of the visible region.

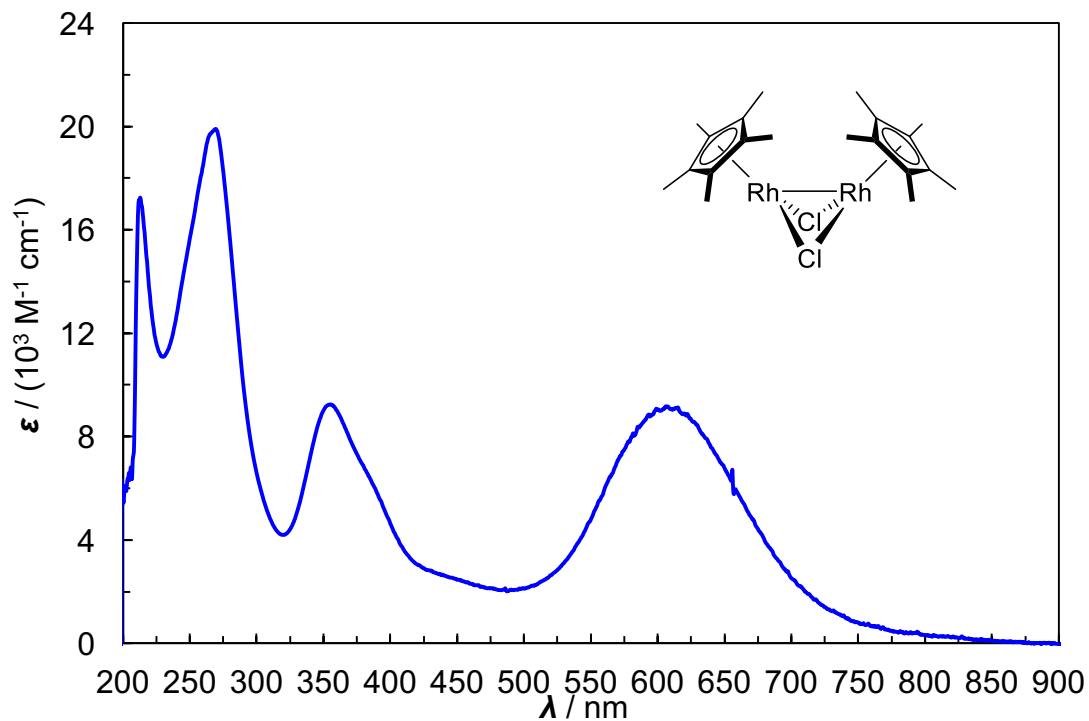


Figure S7. UV-Vis spectrum in THF of $[\text{Cp}^*\text{RhCl}]_2$ from reduction of **3-Cl** with CoCp_2 .

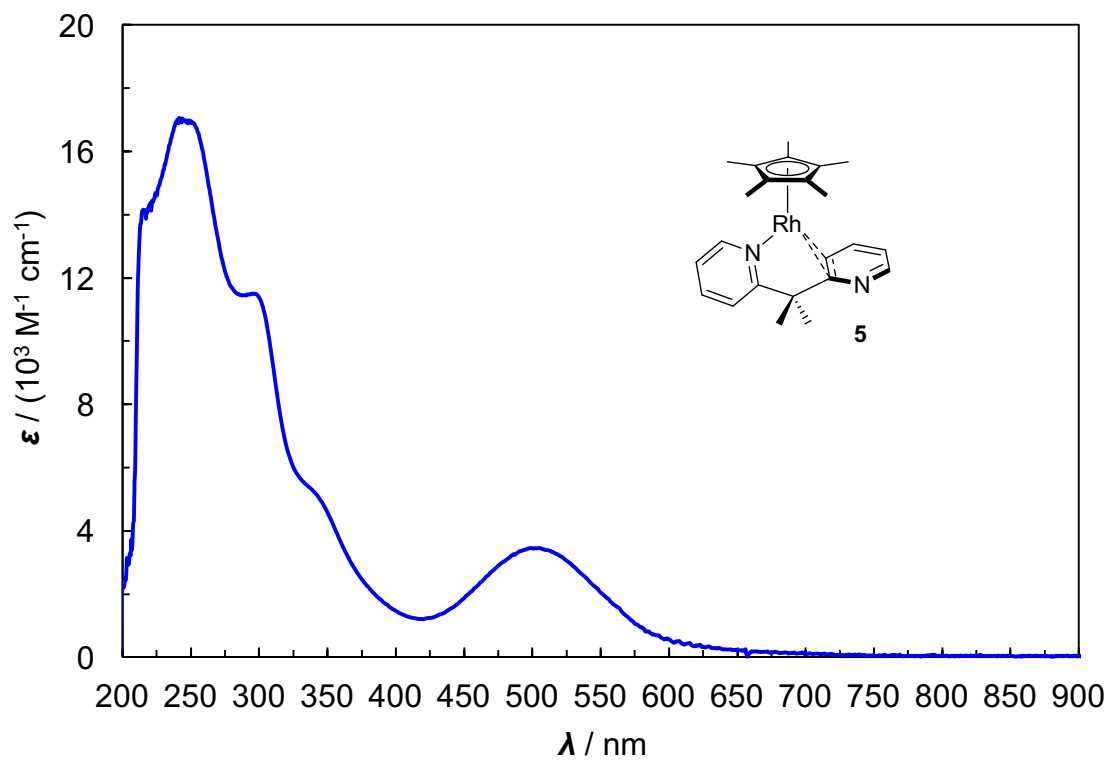


Figure S8. UV-Vis spectrum of **5** in THF.

Discussion of UV-Vis Spectroscopy

The electronic absorption spectrum of complex **3-Cl** displays features that are similar to those of bpy analogues, although the sharp features observed around 300 nm ($\epsilon \sim 1.5 \times 10^4 \text{ M}^{-1} \text{ cm}^{-1}$) with bpy-ligated complexes are absent for **3-Cl**.⁶ The $\pi\text{-}\pi^*$ transitions are blueshifted for **3-Cl**, presumably due to the lack of inter-ring conjugation. The charge-transfer bands observed for **3-Cl** between 350-400 nm ($\epsilon \sim 2.5 \times 10^3 \text{ M}^{-1} \text{ cm}^{-1}$) are redshifted for complex **4** (525 nm), consistent with population of higher-lying metal orbitals upon one-electron reduction. The spectrum of complex **6** displays a charge transfer band at 500 nm ($\epsilon \sim 3.5 \times 10^4 \text{ M}^{-1} \text{ cm}^{-1}$), although the differences in geometry and ligand properties (including the presence of a strong π -accepting olefin ligand) make direct comparisons with complexes bearing the $\kappa^2\text{-(}N,N\text{)}$ -bound Me_2dpma ligand difficult. Notably, the spectrum of complex **6** lacks the distinctive features at 700-800 nm observed for **2** and other Rh(I) complexes that are ascribed to transitions involving the conjugated bpy π -system.⁷

NMR Spectra

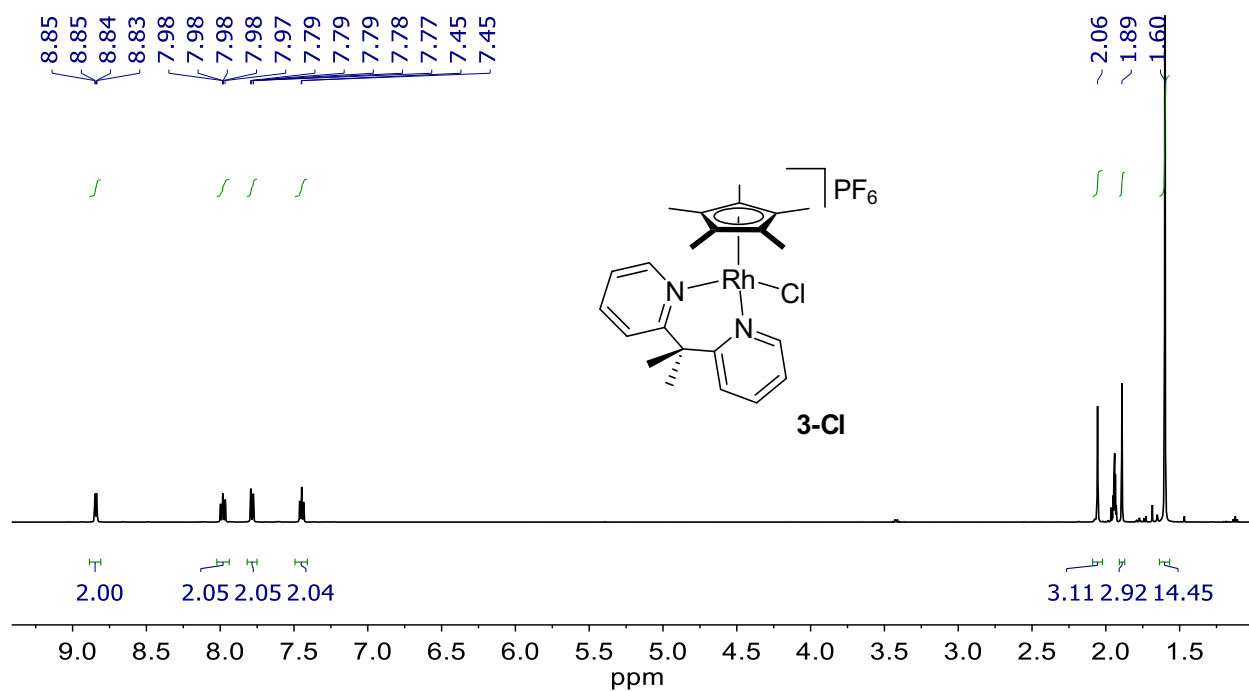


Figure S9. ^1H NMR spectrum (500 MHz, CD_3CN) of **3-Cl**.

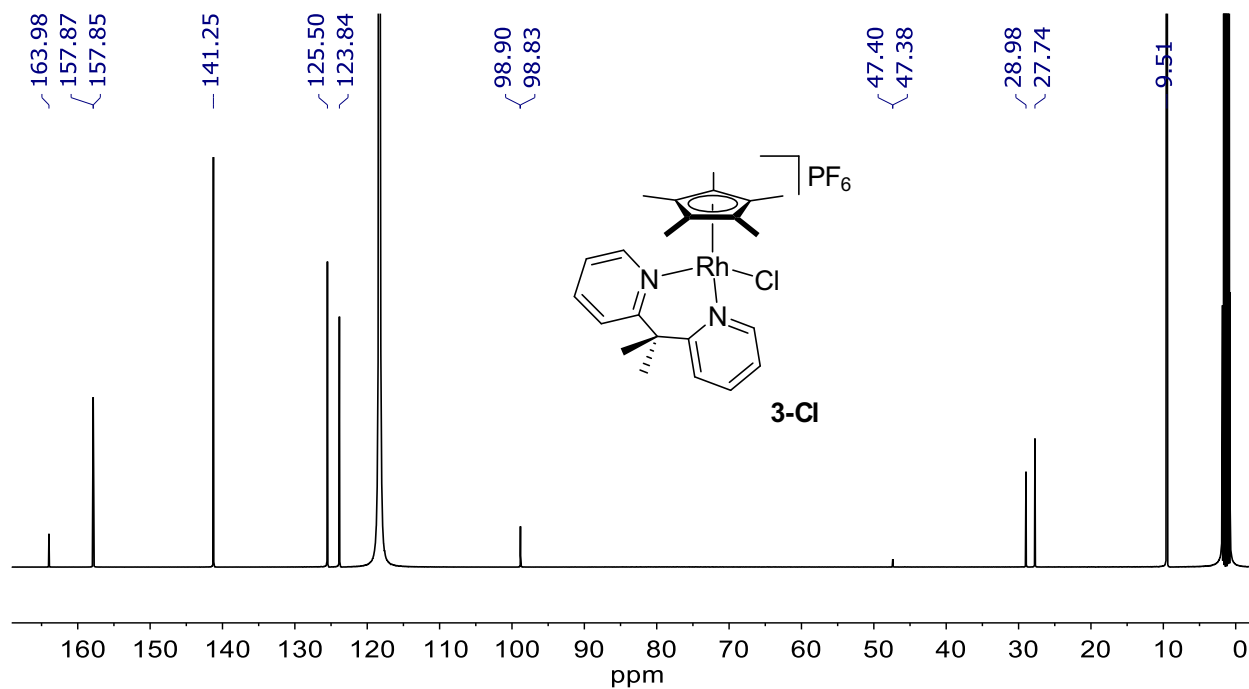


Figure S10. $^{13}\text{C}\{^1\text{H}\}$ NMR spectrum (126 MHz, CD_3CN) of **3-Cl**.

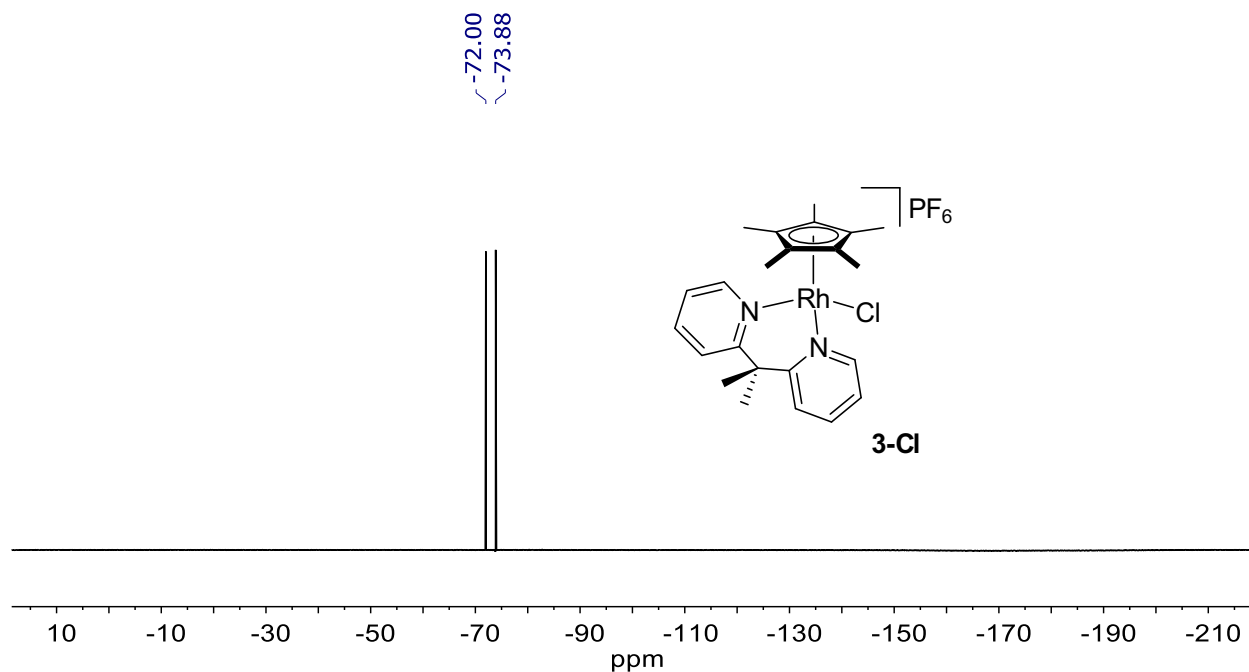


Figure S11. ¹⁹F NMR spectrum (376 MHz, CD₃CN) of **3-Cl**.

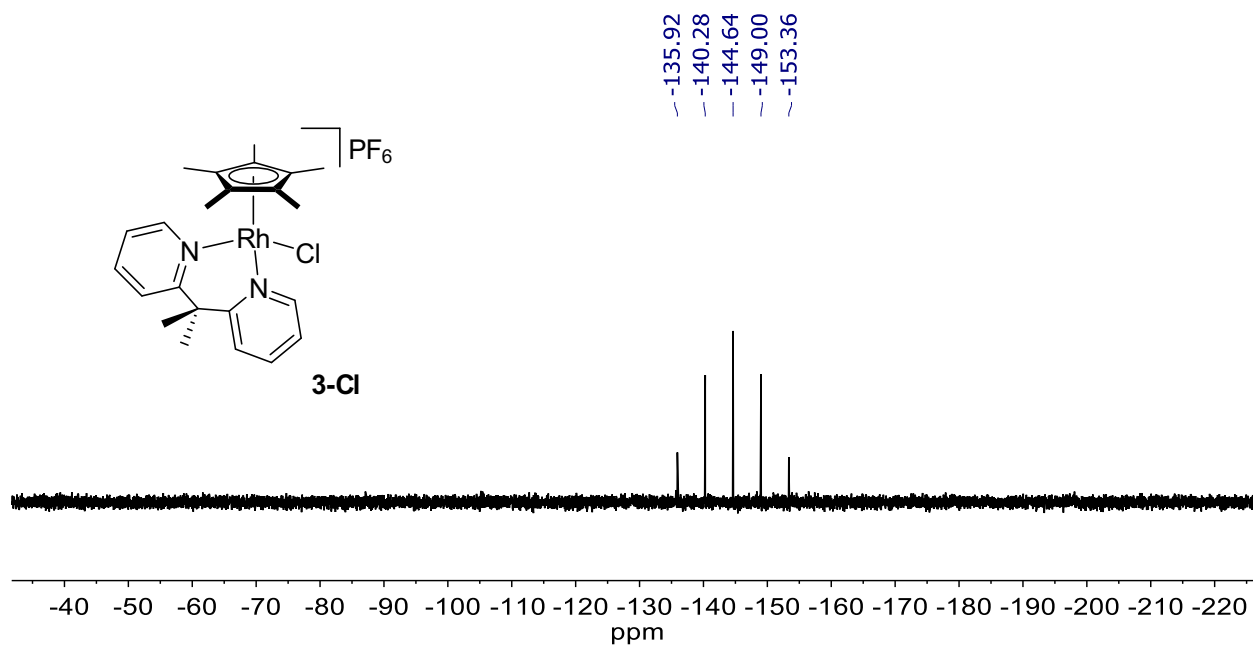


Figure S12. ³¹P{¹H} NMR spectrum (162 MHz, CD₃CN) of **3-Cl**.

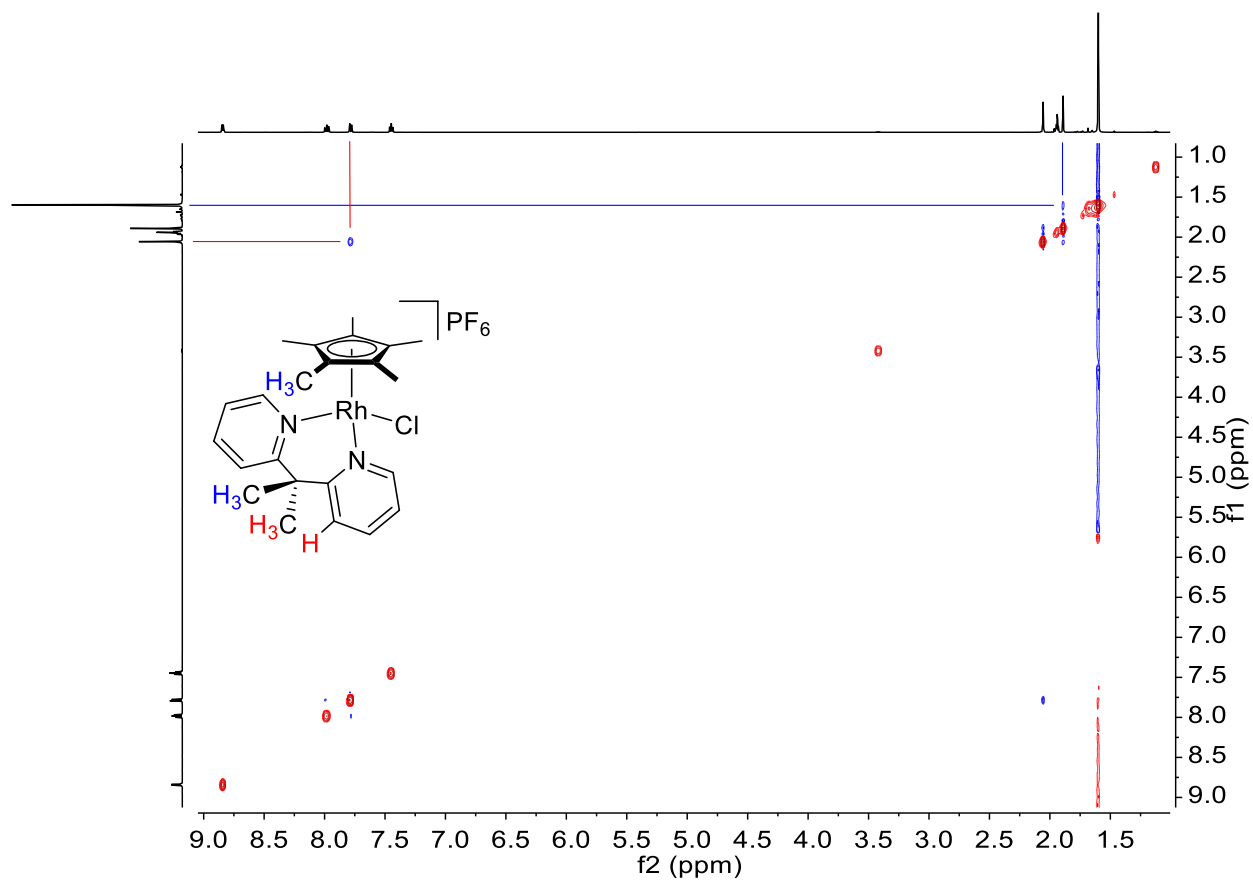


Figure S13. NOESY spectrum (400 MHz, CD₃CN) of **3-Cl**.

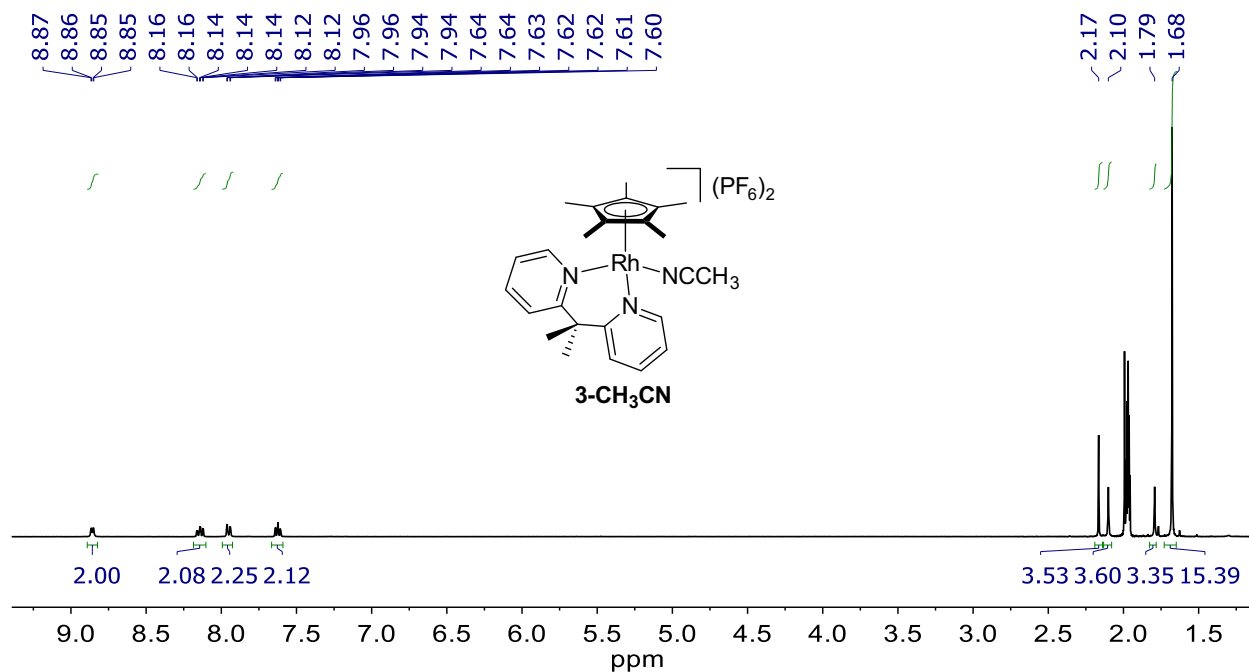


Figure S14. ¹H NMR spectrum (400 MHz, CD₃CN) of **3-CH₃CN**.

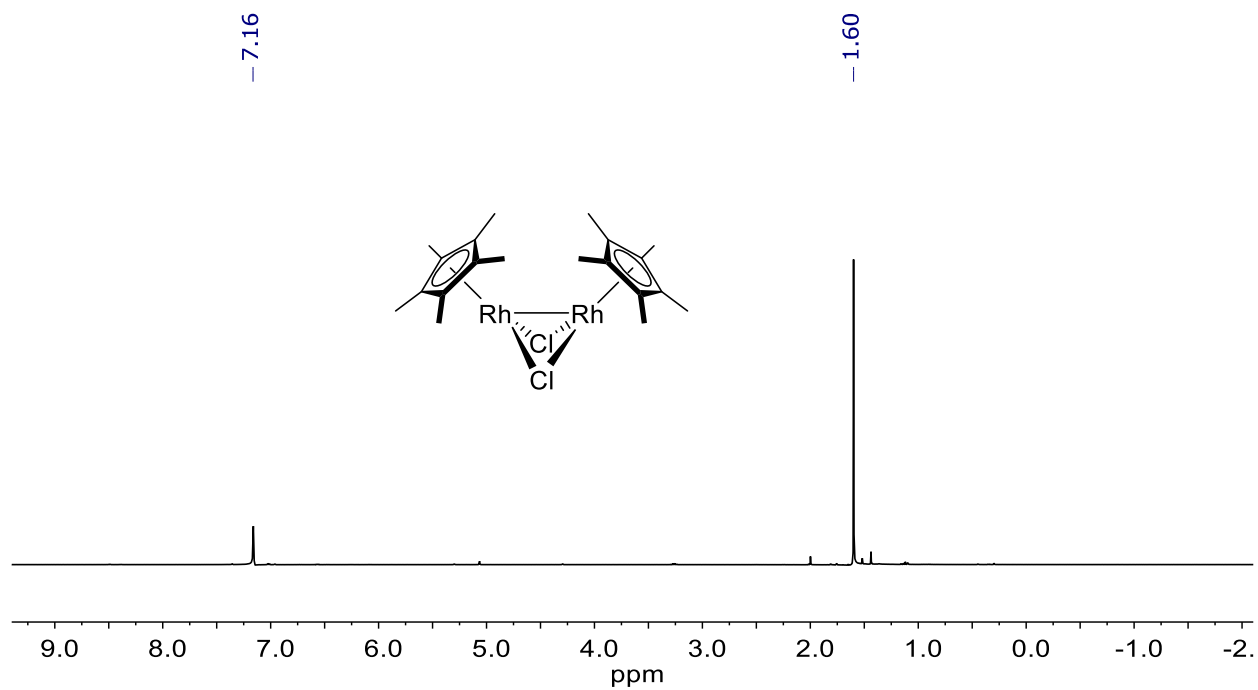


Figure S15. ¹H NMR spectrum (400 MHz, C₆D₆) of **[Cp^{*}RhCl]₂** from Et₂O fraction of the reduction of **3-Cl** with CoCp₂.

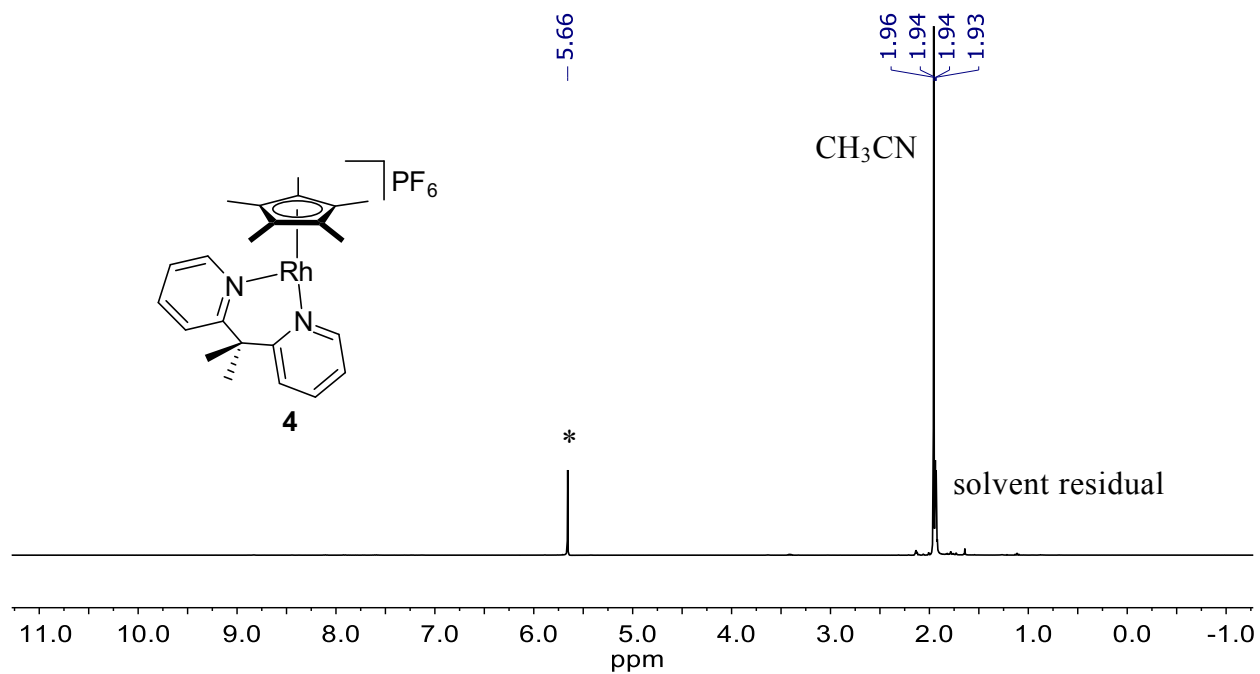


Figure S16. ^1H NMR spectrum (400 MHz, CD_3CN) of **4**. Co-generated $[\text{CoCp}_2][\text{PF}_6]$ marked with (*).

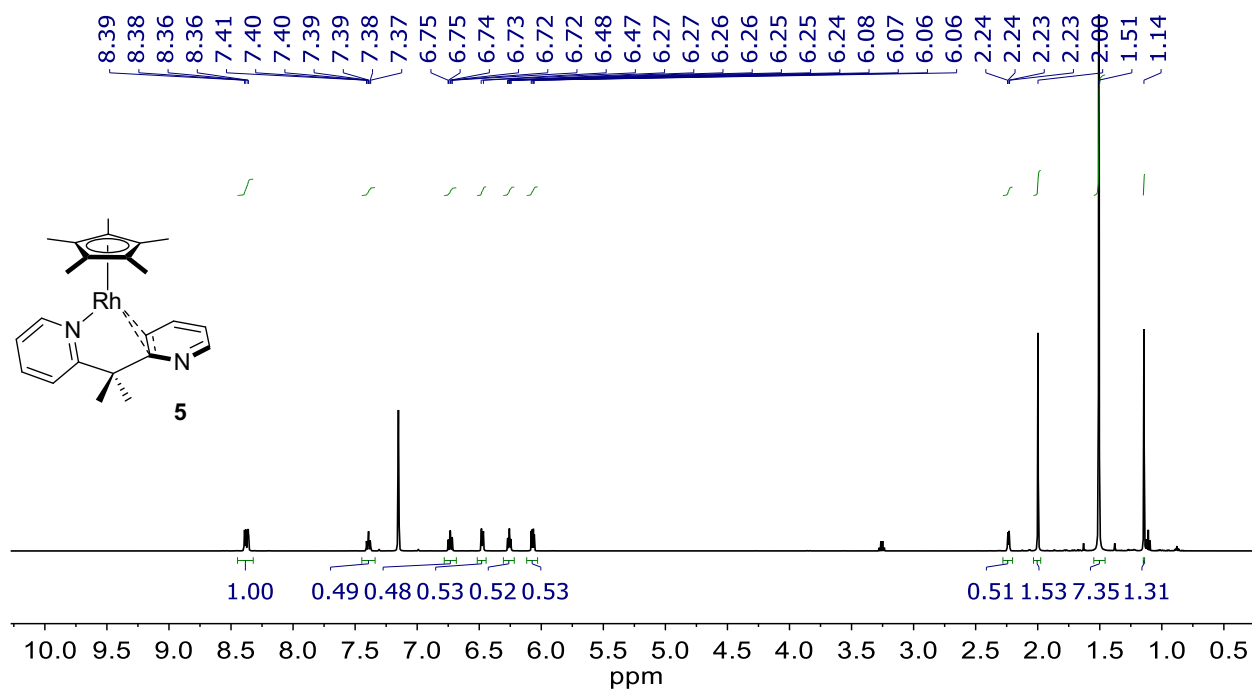


Figure S17. ^1H NMR spectrum (500 MHz, C_6D_6) of **5**.

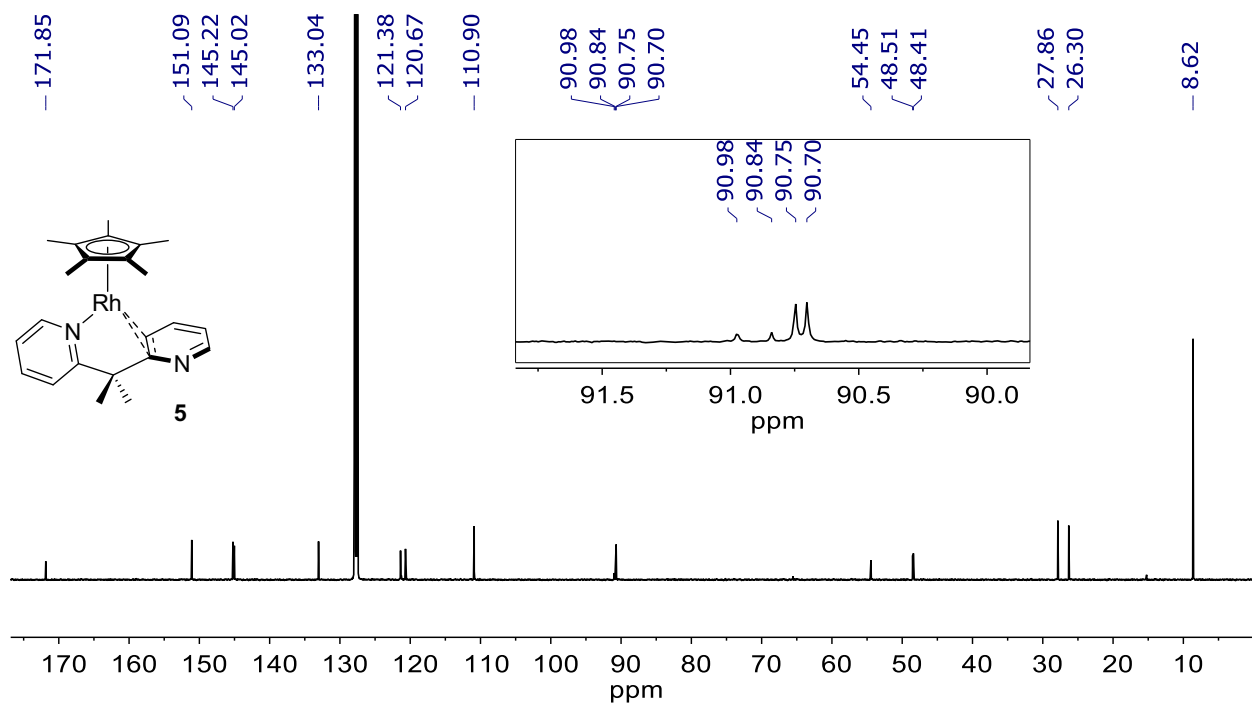


Figure S18. $^{13}\text{C}\{^1\text{H}\}$ NMR spectrum (126 MHz, C_6D_6) of **5**.

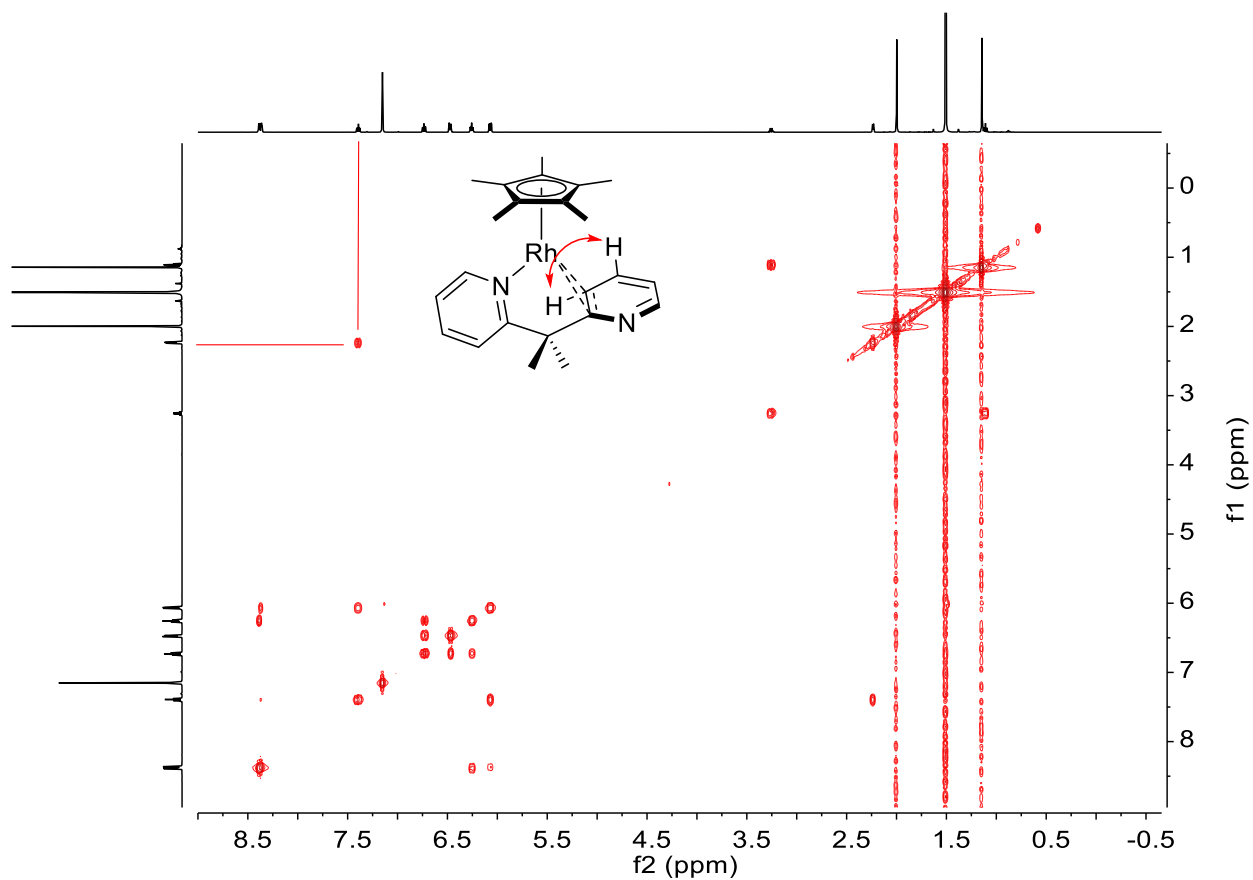


Figure S19. COSY spectrum (400 MHz, C_6D_6) of **5**. The cross-peak at (7.41, 2.24 ppm) indicated coupling between the proton on the pyramidalized carbon C10 and one of the pyridyl protons, consistent with assignment of the peak at 2.25 ppm as the eighth pyridyl proton.

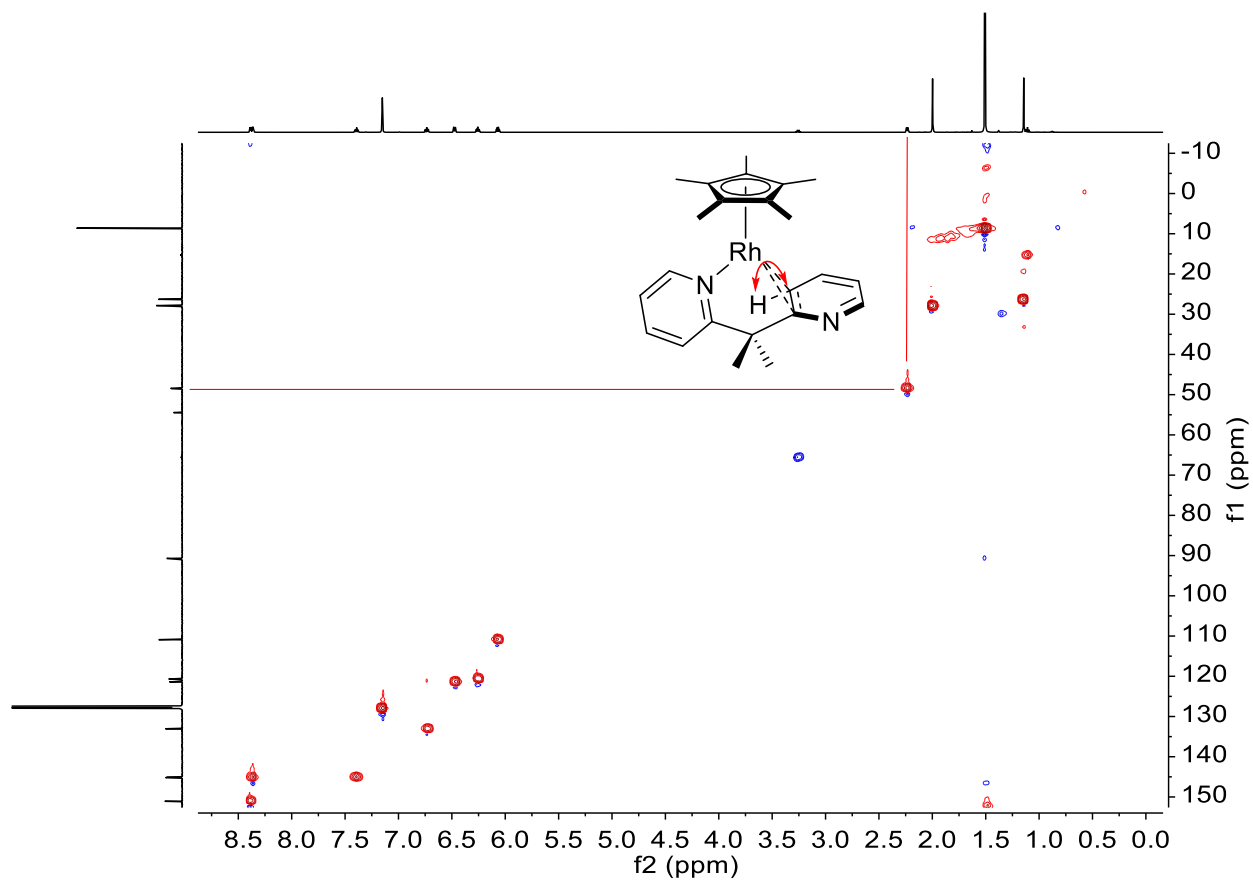


Figure S20. HSQC spectrum (500 MHz, C_6D_6) of **5**. The cross-peak at (2.24, 48.30 ppm) indicated that the upfield-shifted pyridyl proton was bound to one of the carbon atoms displaying C,Rh coupling ($^1J_{\text{C,Rh}} = 12.8$ Hz), consistent with pyramidalization of the carbon atom (C10) resulting in the observed upfield shift in the ^{13}C (48.30 ppm for C10 vs. 121.39 ppm for C4) and ^1H (2.24 ppm for H10 vs. 6.47 ppm for H4).

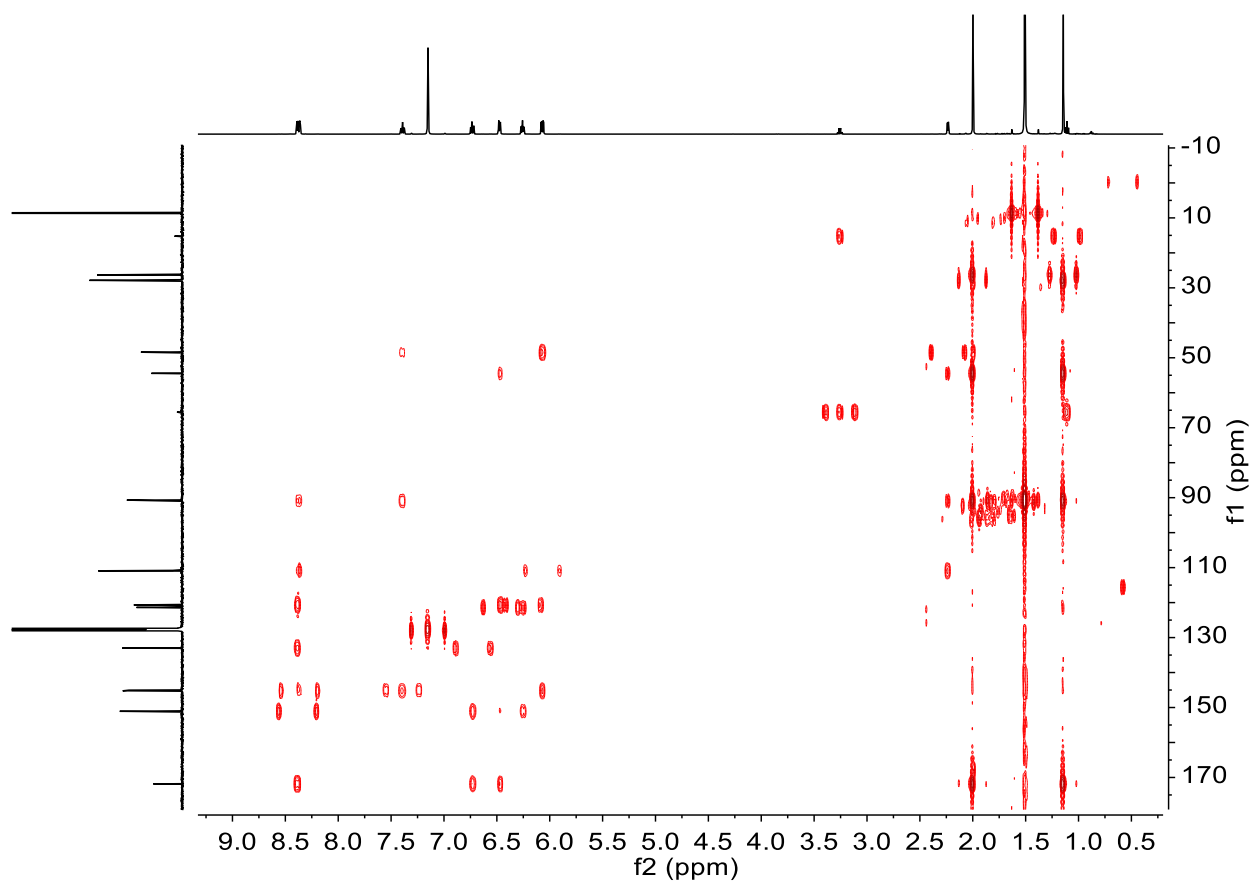


Figure S21. HMBC spectrum (500 MHz, C_6D_6) of **5**. The present spectrum provided the information necessary to assign the ^{13}C resonances corresponding to the carbon atoms in each pyridyl ring. Importantly, this allowed the assignment of the ^{13}C resonance at 90.9 ppm (d, $^1J_{C,Rh} = 16.8\text{Hz}$) to C9 – the *ortho*-pyridyl carbon connected to the $C(CH_3)_2$ bridge – which also displays a substantial upfield shift vs. C5 (171.8 ppm).

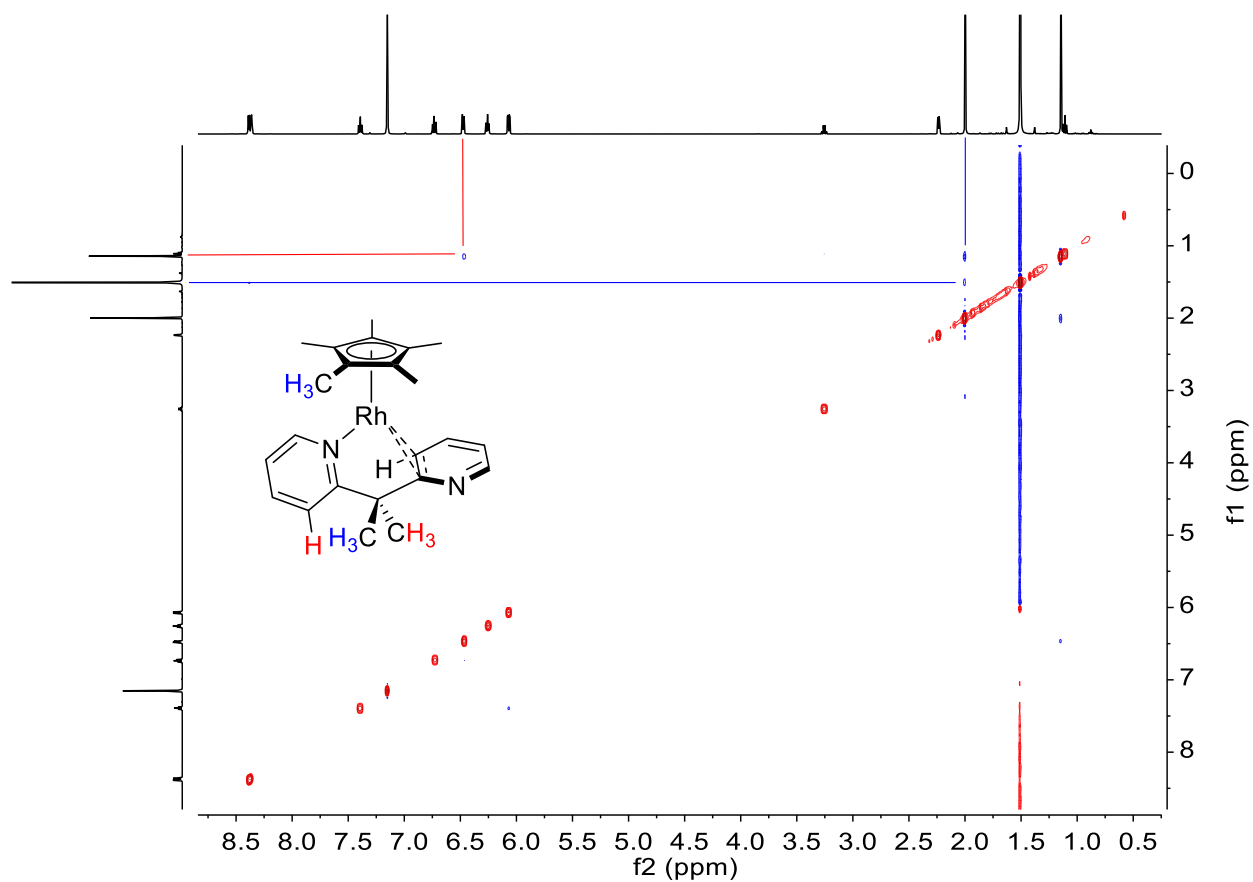


Figure S22. NOESY spectrum (500 MHz, C_6D_6) of **5**. The crosspeaks at (6.47, 1.15 ppm) and (2.00, 1.51 ppm) allowed distinction of the two CH_3 groups on the bridging methylene group.

Crystallographic Information

Data Collection and Refinement Details

Crystals of **4** were thin plates that formed twins by stacking on top of one another. More than two dozen small pieces were cut from these stacked twins before a reasonably single-domain specimen was obtained. Crystals of **3-Cl**, **4** and **5** used for diffraction data collection were mounted on nylon loops using Paratone oil under a nitrogen stream. Low temperature (200 K) data were obtained with X-rays from a Bruker MicroStar microfocus rotating anode generator running at 60 mA and 45 kV (Cu K_{α} = 1.54178 Å; APEX II detector positioned at 50.0 mm and equipped with Helios multilayer mirror optics) for **4** and **5** or with X-rays from a Bruker generator using a fine focus Mo sealed tube running at 30 mA and 50 kV (Mo K_{α} = 0.71073 Å; SMART APEX detector positioned at 50.0 mm and equipped with a MonoCap collimator and graphite monochromator) for **3-Cl**. Longer-than-normal (20 second) counting times were used for the high-angle data frames of **4**. All diffractometer manipulations, including data collection, integration and scaling were carried out using the Bruker APEXII software.⁸ Absorption corrections were applied using SADABS.⁹ Space groups were determined on the basis of systematic absences and intensity statistics and the structures were solved by intrinsic phasing using XT¹⁰ or by direct methods using XS¹¹ (incorporated into SHELXTL) and refined by full-matrix least squares on F^2 . All non-hydrogen atoms were refined using anisotropic displacement parameters. All hydrogen atoms for **3-Cl** were placed in idealized positions and refined using a riding model. The Cp* hydrogen atoms for **4** were also placed in idealized positions and refined using a riding model. The Me₂dpma hydrogens of **4** and all hydrogens of **5** were located from Fourier difference maps and included in the structural models as independent isotropic atoms whose parameters were allowed to vary. The structures were refined (weighted least squares refinement on F^2) to convergence using the Olex software package equipped with XL.¹¹⁻¹²

Table S1. Crystal and Refinement Data

	3-Cl	4	5
CCDC number	1573827	1573828	1573829
empirical formula	C ₂₃ H ₂₉ ClF ₆ N ₂ PRh	C _{23.33} H ₂₉ F ₆ N ₂ PRh	C ₂₃ H ₂₉ N ₂ Rh
formula wt	616.81	585.32	436.39
T (K)	200	200	200
a, Å	8.284 (1)	10.6800(2)	10.8564(2)
b, Å	11.861(2)	11.8136(3)	11.6907(3)
c, Å	25.557(4)	11.8896(3)	16.6402(4)
α, deg	95.308(4)	117.254(2)	90
β, deg	94.332(4)	108.438(2)	103.578 (1)
γ, deg	93.372(3)	97.370(2)	90
V, Å ³	2487.8(6)	1196.94(5)	2052.93(8)
Z	4	2	4
crystal dimensions (mm.)	0.58 × 0.33 × 0.27	0.015 × 0.05 × 0.07	0.14 × 0.11 × 0.07
cryst syst	triclinic	triclinic	monoclinic
space group	P-1 (#2)	P-1 (#2)	P2 ₁ /c (#14)
ρ _{calcd} , g/cm ³	1.647	1.624	1.412
2θ range, deg	3.46 to 66.53	8.80 to 140.58	8.38 to 140.09
completeness to d=0.843Å	99.9	96.4	97.6
wavelength (Å)	0.71073	1.54178	1.54178
reflections collected	38264	19004	20357
indep. reflections/R _{int}	17715/0.033	4268/0.077	3812/0.047
μ, mm ⁻¹	0.92	6.96	6.77
abs corr	Multi-scan	Multi-scan	Multi-scan
GOOF ^c	1.054	1.065	1.049
Data/restraints/parameters	17715/0/627	4268/0/364	3812/0/351
R ₁ , ^a wR ₂ ^b (I > 2σ(I))	0.044, 0.088	0.058, 0.15	0.035, 0.095
R ₁ , ^a wR ₂ ^b (all data)	0.060/0.096	0.069, 0.153	0.037/0.097

$${}^a R_1 = \frac{\sum ||F_o| - |F_c||}{\sum |F_o|} \quad {}^b wR_2 = \left[\frac{\sum [w(F_o^2 - F_c^2)^2]}{\sum [w(F_o^2)^2]} \right]^{1/2} \quad {}^c \text{GOOF} = S = \left[\frac{\sum [w(F_o^2 - F_c^2)^2]}{(n-p)} \right]^{1/2}$$

Refinement Details for 3-Cl.

The asymmetric unit for the solid-state structure of **3-Cl** contained two dicationic Rh(III) moieties and two $[\text{PF}_6]^-$ anions. No special refinement was necessary.

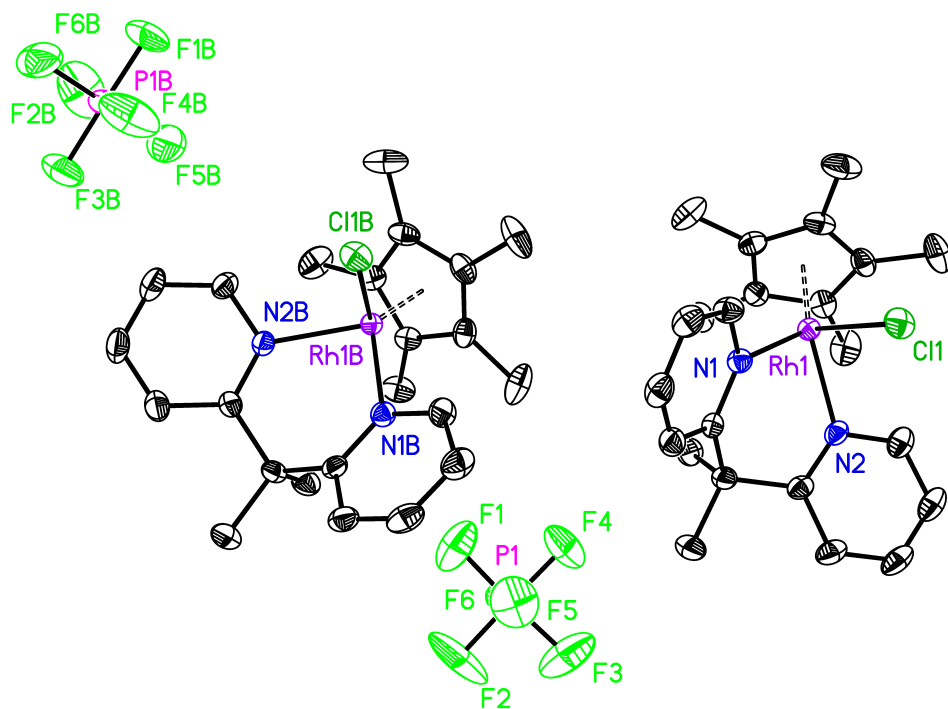


Figure S23. Full solid-state structure of **3-Cl**. Hydrogen atoms omitted for clarity. Displacement ellipsoids shown at the 50% probability level.

Refinement Details for 4.

A weak interaction was observed in the structure of **4** between the Rh center and the C7–H7A methyl group bond on the Me₂dpma ligand backbone (Rh•••H7A: 2.46(6) Å; Rh•••C7: 3.199(6) Å). A marginally significant deformation of the methyl group, consistent with this interaction, is observed: an elongated 1.18(7) Å C7–H7A bond (cf. C7–H7B: 0.94(10) and C7–H7C: 0.84(7) Å) along with an expanded 121(3)° C6–C7–H7A bond angle and a contracted 92(7)° H7B–C7–H7C angle. This deformation of the C7 methyl group was responsible for three of the B-level alerts raised by the CheckCIF program.

Additionally, a disordered component was observed in the cavity between two symmetry-related molecules of **4** near the inversion center at (1, 0, 1) in the unit cell. The largest difference Fourier peak for this component was refined isotropically with a variable occupancy factor as a C atom (C1S). The occupancy of C1S refined to a value of 0.33 and was 1.10 Å from its symmetry-related mate, indicating only partial occupation of this cavity by an unknown component, likely a CH₃CN solvent molecule.

Two other B-level alerts were raised by the CheckCIF program due to the presence of residual electron density near the Rh center. This observation is likely due to the weak high-angle data resulting from the very small crystal that had to be used in this study and to the high electron density associated with the Rh metal center. This information was included in the final .cif file to explain the CheckCIF alerts.

Least-squares refinement cycles that rejected increasing amounts of (the weaker) high-angle data progressively decreased the residual electron density near the Rh atom but had little effect on the C7 methyl geometry. With data beyond $2\theta = 105^\circ$ rejected, CheckCIF B-alerts for high residual electron density near Rh did not occur.

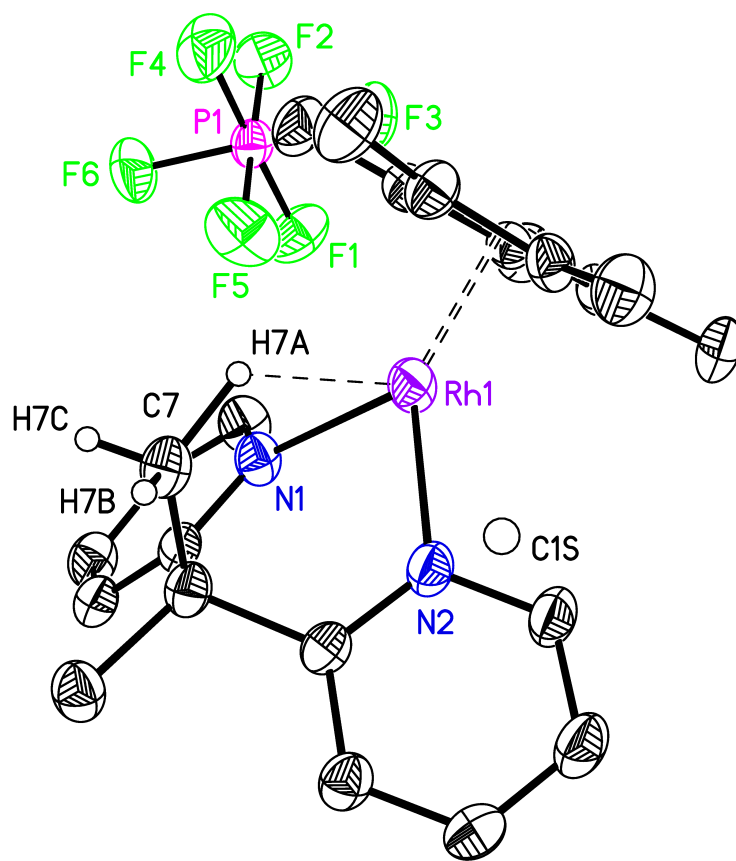


Figure S24. Full solid-state structure of **4**. Hydrogen atoms (except those for methyl carbon C7) omitted for clarity. Displacement ellipsoids shown at the 50% probability level.

Refinement Details for 5.

To confirm the presence of a hydrogen atom on carbon C10, an idealized hydrogen was not calculated at this position. Electron density near C10 but not nitrogen N2 was observed in the Fourier difference map, consistent with the presence of a hydrogen atom on C10. H10 was therefore included in the model as an isotropic atom and its position was refined freely. No other special refinement was necessary.

Pyramidalization of C9 and C10 is evident by displacements of these atoms by 0.24 and 0.18 Å, respectively, from the mean planes of their three contiguous (covalently-bonded) neighbor atoms. This situation contrasts with non-pyramidalized C5, which is displaced from the analogous mean plane by 0.05 Å.

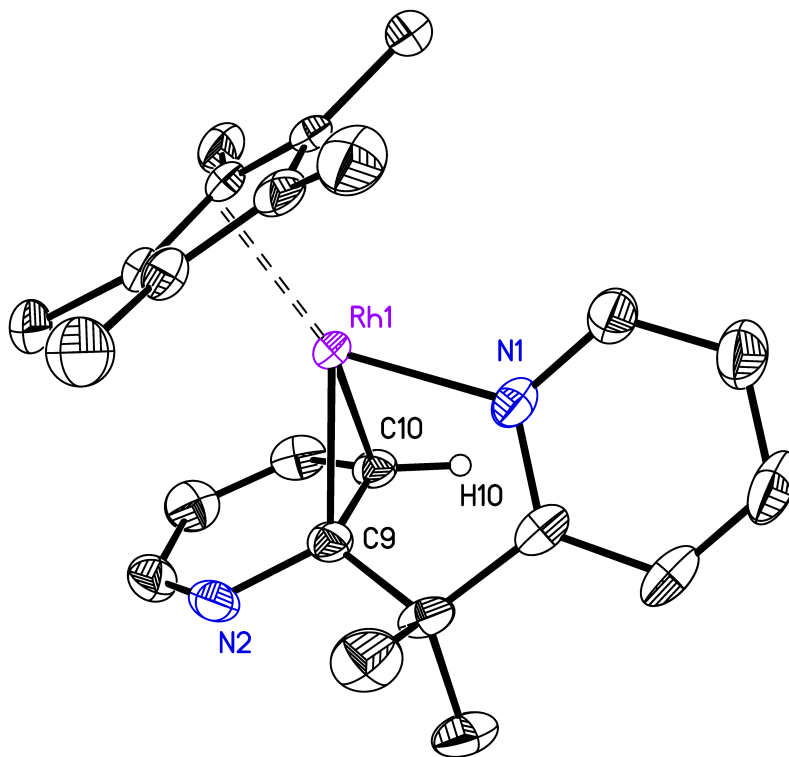


Figure S25. Full solid-state structure of **5**. Hydrogen atoms except for H10 omitted for clarity. Displacement ellipsoids shown at the 50% probability level.

TableS2: Relevant Structural Parameters

Complex	3-Cl ^a	4	5
Rh–Cp* ^b	1.803 Å 1.803 Å	1.827 Å	1.885 Å
Avg. Rh–(C ₅ (CH ₃) ₅)	2.175 Å 2.175 Å	2.195 Å	2.245 Å
Avg. Rh–(C ₅ (CH ₃) ₅)	3.320 Å 3.316 Å	3.312 Å	3.365 Å
Rh–N1	2.130(2) Å 2.129(2) Å	2.096(4) Å	2.064(2) Å
Rh–N2	2.133(2) Å 2.122(2) Å	2.100(4) Å	-
Rh–C9	-	-	2.105(3) Å
Rh–C10	-	-	2.144(2) Å
C9–C10	1.398(3) Å 1.390(3) Å	1.395(7) Å	1.467(4) Å
Rh–Cl	2.4134(7) Å 2.4105(6) Å	-	-
∠(N1–Rh–N2)	85.44(8)° 85.58(8)°	86.34(17)°	

^a two independent molecules observed in the asymmetric unit cell; ^b distance between the Rh center and the calculated centroid of the Cp* ring.

References

- (1) (a) White, C.; Yates, A.; Maitlis, P. M. *Inorg. Synth.* **1992**, *29*, 228; (b) Vedernikov, N.; Miftakhov, R.; Borisoglebski, S. V.; Caulton, K. G.; Solomonov, B. N. *Chem. Heterocycl. Compd.* **2002**, *38*, 406.
- (2) Fulmer, G. R.; Miller, A. J. M.; Sherden, N. H.; Gottlieb, H. E.; Nudelman, A.; Stoltz, B. M.; Bercaw, J. E.; Goldberg, K. I. *Organometallics* **2010**, *29*, 2176.
- (3) (a) Harris, R. K.; Becker, E. D.; De Menezes, S. M. C.; Goodfellow, R.; Granger, P. *Pure Appl. Chem.* **2001**, *73*, 1795; (b) Harris, R. K.; Becker, E. D.; De Menezes, S. M. C.; Granger, P.; Hoffman, R. E.; Zilm, K. W. *Pure Appl. Chem.* **2008**, *80*, 59.
- (4) (a) Sharp, P. R.; Hoard, D. W.; Barnes, C. L. *J. Am. Chem. Soc.* **1990**, *112*, 2024; (b) Hoard, D. W.; Sharp, P. R. *Inorg. Chem.* **1993**, *32*, 612.
- (5) Bockman, T. M.; Chang, H. R.; Drickamer, H. G.; Kochi, J. K. *J. Phys. Chem.* **1990**, *94*, 8483.
- (6) Henke, W. C.; Lionetti, D.; Moore, W. N. G.; Hopkins, J. A.; Day, V. W.; Blakemore, J. D. *ChemSusChem* **2017**, *10*, 4589.
- (7) Lionetti, D.; Day, V. W.; Blakemore, J. D. *Organometallics* **2017**, *36*, 1897.
- (8) *APEX2, Version 2 User Manual, M86-E01078*; Bruker Analytical X-ray Systems: Madison, WI, June 2006.
- (9) SADABS (version 2008/1): Program for Absorption Correction for Data from Area Detector Frames
- (10) Sheldrick, G. *Acta Crystallogr., Sect. A: Found. Crystallogr.* **2015**, *71*, 3.
- (11) Sheldrick, G. *Acta Crystallogr., Sect. C: Cryst. Struct. Commun.* **2015**, *71*, 3.
- (12) Dolomanov, O. V.; Bourhis, L. J.; Gildea, R. J.; Howard, J. A. K.; Puschmann, H. *J. Appl. Crystallogr.* **2009**, *42*, 339.